Quantum field heat engine powered by phonon-photon interactions

Alessandro Ferreri,[1,2] Vincenzo Macrì,[2,3] Frank K. Wilhelm,[1] Franco Nori,[2,4,5] and David Edward Bruschi[1]

[1] *Institute for Quantum Computing Analytics (PGI-12), Forschungszentrum Jülich, 52425 Jülich, Germany*
[2] *Theoretical Quantum Physics Laboratory, RIKEN, Wako-shi, Saitama 351-0198, Japan*
[3] *Dipartimento di Ingegneria, Università degli Studi di Palermo, Viale delle Scienze, 90128 Palermo, Italy*
[4] *Center for Quantum Computing, RIKEN, Wako-shi, Saitama 351-0198, Japan*
[5] *Physics Department, The University of Michigan, Ann Arbor, Michigan 48109-1040, USA*

(Received 19 May 2023; accepted 29 November 2023; published 21 December 2023)

We present a quantum heat engine based on a cavity with two oscillating mirrors that confine a quantum field. The engine performs an Otto cycle during which the walls and a field mode, together representing the working substance of the engine, interact via a nonlinear Hamiltonian. Resonances between the frequencies of the cavity mode and the walls allow one to transfer heat from the hot and the cold bath by exploiting the conversion between phononic and photonic excitations. We study the time evolution of the system and show that net work can be extracted after a full cycle. We evaluate the efficiency of the process.

DOI: 10.1103/PhysRevResearch.5.043274

I. INTRODUCTION

Quantum thermodynamics studies physical processes at the quantum scale through the lens of thermodynamics [1–3]. The overall aim of this field of research is to extend concepts initially developed in the classical theory, such as heat, work, and thermodynamic efficiency, into the quantum domain where purely quantum features can be exploited [4,5]. These include quantum correlations [6], quantum coherence [7], and vacuum fluctuations [8,9]. One task is to propose and characterize novel thermodynamic cycles by taking advantage of the nonclassical nature of the working substance to extract work for different tasks [10–12]. The interest in studying thermodynamical cycles at the quantum level goes beyond the mere possibility of reaching higher degrees of efficiency but aims towards miniaturization of future thermal machines based on quantum systems.

The quantum Otto cycle is a thermodynamic cycle that enjoys relative ease of theoretical implementation in a quantum framework compared to other cycles, especially if implemented in cavity optomechanics [13–18]. It consists of a combination of two thermodynamic "strokes": (i) the *isochoric transformation*, performed by maintaining constant the spacing of the energy levels of the system during thermalization with the bath; (ii) the *adiabatic* transformation, where the thermally isolated system evolves with the total number of excitations kept constant. A time optimization of the latter benefits the performance of the heat engine in the generation of output power [19,20]. Also for this reason, such a simple cycle has been implemented and studied in the context of finite-time Otto cycles [21–23], Otto-engine power generation [24–26], heat engines with interacting systems [27], and quantum heat engines based on phononic fields in Bose-Einstein condensates [28].

In this work we study the quantum Otto cycle in the context of quantum optomechanics [29]. The system consists of a cavity-optomechanical setup where two movable mirrors confine a quantum field. The mirror and field modes strongly interact via phonon-photon vacuum fluctuations and the mirrors are also coupled individually to a thermal bath. We employ our system to show that the proposed quantum field heat engine can generate power in finite time after each cycle and we estimate the efficiency of such a process. We note that the platforms considered here have already allowed for the experimental observation of thermal-phonon hopping, i.e., the exchange of thermal energy between individual phonon modes [30].

In the quantum Otto cycle under consideration, the working substance consists of three interacting subsystems: these are the two movable walls (whose quantized position determines a quantum degree of freedom for each wall) and the confined quantum electromagnetic field. While the two movable walls individually interact with the hot and the cold bath, the cavity mode does not interact with any of these baths directly, but only through the mediation of the respective wall. More precisely, each wall is connected to a single thermal bath: the first wall (called W1) interacts with a *cold* bath at temperature T_{c}, while the second wall (called W2) interacts with a *hot* bath at temperature T_{h}. The transfer of thermal excitations from the bath to the cavity mode occurs whenever the frequency of the cavity is resonant with the frequency of the corresponding wall. The field modes are driven by an external drive that controls the length of the cavity.

We stress that the photon-phonon interaction occurs beyond linearization, thereby retaining the dynamical-Casimir-like three-body terms in the Hamiltonian [31–36], with the

Published by the American Physical Society under the terms of the Creative Commons Attribution 4.0 International license. Further distribution of this work must maintain attribution to the author(s) and the published article's title, journal citation, and DOI.

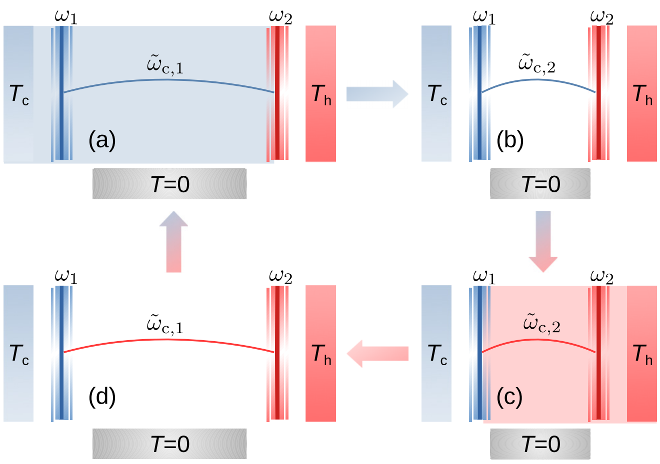

FIG. 1. Pictorial representation of the cavity performing the quantum Otto cycle: two movable walls, coupled to two baths at different temperatures, confine a cavity mode, which is weakly coupled to a bath at $T \simeq 0$. The four panels describe the four strokes of the cycle: (a) cold isochoric, (b) adiabatic compression, (c) hot isochoric, and (d) adiabatic expansion.

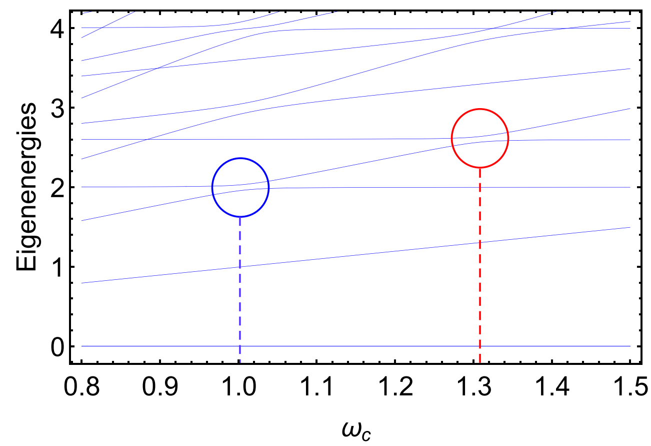

FIG. 2. Lowest-energy levels of the system Hamiltonian as a function of ω_c. Circles highlight the avoided levels in which the dressed resonances (blue) $\omega_1 = 2\omega_{c,1}$ and (red) $\omega_2 = 2\omega_{c,2}$ occur. For each resonance condition, the effective cavity frequency $\tilde{\omega}_c$ was estimated. Here $\tilde{\omega}_{c,1} = 1.01$, $\tilde{\omega}_{c,2} = 1.31$, $\omega_1 = 2$, $\omega_2 = 2.6$, and $g_1 = g_2 = 0.05$. Frequencies are normalized with respect to the bare frequency of the cavity mode $\omega_{c,1}$.

ambition of characterizing the thermodynamic performance of the system in its full nonlinear regime. This includes also the multimode character of the interaction [37]. Moreover, in contrast to standard studies of four-stroke thermal machines that consider the single strokes separately, we employed the master equation formalism in order to run two consecutive cycles as a function of time. The need for the master equation approach throughout the whole dynamics is explained by the fact that we effectively change the length of the cavity in a time-dependent way through the external drive, thereby controlling the heat transfer between the cavity and the baths through the walls.

II. QUANTUM MODEL

The system is composed of two movable walls that confine an uncharged massless scalar quantum field and interact with a local bath. Our choice of field is a good approximation for a single-polarization version of a confined electromagnetic spin-1 field [38]. We further simplify the setup by considering a one dimensional cavity, which allows us to obtain the system Hamiltonian $\hat{H}_s$ following the standard procedure of solving the classical field equations and then quantizing [34] (see also Appendix A). The system is schematically represented in Fig. 1.

The Hamiltonian can be split as usual as $\hat{H}_s = \hat{H}_0 + \hat{H}_I$, where $\hat{H}_0 = \omega_1 \hat{b}_1^\dagger \hat{b}_1 + \omega_2 \hat{b}_2^\dagger \hat{b}_2 + \omega_c \hat{a}^\dagger \hat{a}$ is the bare Hamiltonian and H_I is the interaction Hamiltonian. The latter has been previously obtained [29] and reads

$$\hat{H}_I = \frac{g_1}{2}(\hat{a} + \hat{a}^\dagger)^2(\hat{b}_1 + \hat{b}_1^\dagger) + \frac{g_2}{2}(\hat{a} + \hat{a}^\dagger)^2(\hat{b}_2 + \hat{b}_2^\dagger). \quad (1)$$

Here, $\hat{a}, \hat{a}^\dagger$ are the photonic operators for the cavity-field mode, while $\hat{b}_j, \hat{b}_j^\dagger$ $(j = 1, 2)$ are the phononic operators for the walls-field mode. The operators satisfy the canonical commutator relations $[\hat{a}, \hat{a}^\dagger] = 1$ and $[\hat{b}_j, \hat{b}_{j'}^\dagger] = \delta_{jj'}$. Furthermore, ω_j are the frequencies of the two movable walls ($\omega_1 < \omega_2$ for convenience), whereas ω_c is the frequency of the cavity field mode. In addition, the coupling constants g_j quantify the strength of the coupling between the field mode and the jth wall (see Appendix A). Finally, eigenvalues and states will be labeled by $l, m, n \in \mathbb{N}$, which stand for l excitations of the field mode, m excitations of W1, and n excitations of W2. Throughout this work we assume that $\hbar = c = k_B = 1$.

The interaction Hamiltonian Eq. (1) contains three types of terms as follows. (i) The radiation pressure $\hat{a}^\dagger \hat{a}(\hat{b}_j + \hat{b}_j^\dagger)$, paramount in standard optomechanics [39,40], which shifts the cavity frequency ω_c in case of coherent motion of the wall. (ii) The excitation transfer terms $\hat{a}^2 \hat{b}_j^\dagger + (\hat{a}^\dagger)^2 \hat{b}_j$, which convert single-phonon excitations into photon pairs (and vice versa). In other words, they convert mechanical and electromagnetic energy into each other. In order for the photons to appear and contribute during the dynamics, resonance conditions $k\omega_j = 2\omega_c$ with $k \in \mathbb{N}$ involving high-frequency movable walls must be fulfilled [33]. Such resonances can be achieved in current optomechanical setups using real movable mirrors [30,41]. However, they play the most significant role in experimental platforms based on superconducting circuits [42–45]. (iii) The counter-rotating terms $\hat{a}^2 \hat{b}_j + (\hat{a}^\dagger)^2 \hat{b}_j^\dagger$, which generally contribute to modifying the energy density of the cavity field (because of the quantum wall fluctuations [32]). They are also responsible for the nonconservation of the particle number and, in the ultrastrong regime, the presence of quantum correlations [46]. Counter-rotating terms are involved in virtual processes that would allow one to observe higher-order coherent processes in cavity optomechanics [47,48].

The interaction between the bosonic modes not only inevitably alters the structure of the energy levels with respect to the bare ones, but it also lifts the degeneracy in the presence of resonances. To this end we diagonalize the Hamiltonian H_s numerically and plot the energy levels in Fig. 2 for different values of the frequency ω_c. The figure clearly shows the presence of avoided level crossings due to the energy split in proximity of the frequency values $\omega_{c,1} = \omega_1/2$ and $\omega_{c,2} = \omega_2/2$, i.e., where the resonances are expected to occur as discussed above. The dashed vertical lines in Fig. 2 highlight the shift in the bare frequencies. The effective cavity frequencies $\tilde{\omega}_{c,i}$ $(i = 1, 2)$ involved in the coherent resonant processes can be estimated numerically by calculating the minimal splitting of the avoided level crossings.

We use open quantum system dynamics to compute all quantities of interest [49]. This requires us to solve the master equation for the density operator $\hat{\rho}$ representing the state. Since we are considering a strongly interacting system, we employ tools developed in the literature [34,50,51]. In particular, we employ the Lindblad equation $\dot{\hat{\rho}} = -i[\hat{H}, \hat{\rho}] + \hat{\mathcal{L}}_D\hat{\rho}$, where $\hat{\mathcal{L}}_D$ indicates the Lindblad superoperator expressed in the dressed base (see Appendix B). Here we assume that the three subsystems are coupled to three different baths: W1 is coupled to a cold bath with damping rate γ_1 and temperature T_c; W2 is coupled to a hot bath with damping rate γ_2 and temperature $T_h > T_c$; the cavity mode interacts with its own bath with damping rate $\kappa \simeq 0$ and temperature $T \simeq 0$. Note that low damping rates in platforms based on cavity resonators are achievable with the current state of art of the technology [52–55].

III. QUANTUM OTTO CYCLE

The main idea of this work is to exploit the mechanical-electromagnetic energy conversion to perform the quantum Otto cycle using the two walls as bosonic channels, thereby facilitating the heat transfer between the hot and cold baths through the cavity mode. We present here the framework employed to achieve our goal.

Any heat engine can be characterized by evaluating the output power $\mathcal{P}$ and the efficiency η of a single thermodynamic cycle. Thus we consider the total Hamiltonian $\hat{H}_{\rm tot}(t) = \hat{H}_s + \hat{H}_{\rm dr}(t)$ that includes the time-dependent drive term $\hat{H}_{\rm dr}(t)$. This contribution is expressed in the dressed picture and periodically drives the cavity frequency from $\tilde{\omega}_{c,1}$ to $\tilde{\omega}_{c,2}$ and vice versa, simulating the physical process of compression and expansion of the cavity. This can be understood from the fact that the frequency of a trapped field mode decreases or increases by respectively increasing or reducing the length of the cavity. Thus changes in frequency simulate changes in length. Concretely, we have $\hat{H}_{\rm dr}(t) = f(t)\Delta\omega\hat{A}^\dagger\hat{A}$, where $\Delta\omega = \tilde{\omega}_{c,2} - \tilde{\omega}_{c,1}$ is the dressed-frequency difference, $\hat{A}, \hat{A}^\dagger$ are the cavity dressed operators obtained by diagonalizing the Hamiltonian, and $f(t)$ is a periodic smooth step function (see Appendix C). Such functions are commonly employed in circuit quantum electrodynamics (QED) [56–61]. Furthermore, time-dependent drives have also been considered in studies of nonlinear optomechanics [62–64].

In order to investigate the thermodynamic features of the system, we define the change of internal energy $\Delta\mathcal{U}(t) = \mathrm{Tr}[\hat{H}_{\rm tot}(t)\rho(t)] - \mathrm{Tr}[\hat{H}_{\rm tot}(0)\rho(0)]$, the change in heat $\mathcal{Q}(t) = \int_0^t d\tau\, \mathrm{Tr}[\hat{H}_{\rm tot}(\tau)\dot{\rho}(\tau)]$, and the change in work $\mathcal{W}(t) = \int_0^t d\tau\, \mathrm{Tr}[\dot{\hat{H}}_{\rm tot}(\tau)\rho(\tau)]$. These three quantities satisfy the first law of thermodynamics in its quantum formulation:

$$\Delta\mathcal{U}(t) = \mathcal{Q}(t) + \mathcal{W}(t). \tag{2}$$

We then provide a formal definition for the output power $\mathcal{P}$ and the efficiency η of a thermodynamical process as

$$\mathcal{P} := \frac{d}{dt}\mathcal{W}(t), \quad \eta := -\frac{\mathcal{W}^{\rm out}}{\mathcal{Q}^{\rm in}}, \tag{3}$$

where $\mathcal{W}^{\rm out}$ and $\mathcal{Q}^{\rm in}$ are, respectively, the work provided and the heat absorbed by the system. These are the main expressions evaluated in our work.

We now present our quantum Otto cycle, which is composed of a preliminary phase and four steps as follows. (0) *Initialization*: the working substance is prepared in its vacuum state $\rho(0) = |0\rangle\langle 0|$ and we assume that the cavity is initially coupled to W1 by means of the resonance condition $\omega_{c,1} = \omega_1/2$ (see Fig. 1). (a) *Cold isochoric*: thermal cold phonons from W1 are converted into photons, until the subsystem W1 + cavity is thermalized. (b) *Adiabatic compression*: the external drive quickly shifts the field frequency from $\tilde{\omega}_{c,1}$ to $\tilde{\omega}_{c,2}$, thereby ensuring the classical adiabaticity of the process (see Appendix C). (c) *Hot isochoric*: the newly activated resonance $\omega_{c2} = \omega_2/2$ facilitates the excitation transfer between the cavity mode and W2, during which hot phonons are converted into photons. (d) *Adiabatic expansion*: the drive changes the cavity mode frequency back to the resonance regime $\omega_{c,1} = \omega_1/2$. After this step, the system is ready to restart from the *cold isochoric* stroke of step (a).

A. Analysis of the dynamics

We have solved numerically the master equation and therefore calculated the time evolution of the average internal energy $\Delta\mathcal{U}(t)$ directly, while we have computed the average work $\mathcal{W}(t)$ by integrating the expression of the power $\mathcal{P}(t) \equiv \mathrm{Tr}[\rho(t)\dot{\hat{H}}_{\rm tot}(t)] = \mathrm{Tr}[\rho(t)\dot{\hat{H}}_{\rm dr}(t)] = \dot{f}(t)\Delta\omega\mathrm{Tr}[\rho(t)\hat{A}^\dagger\hat{A}]$ defined in Eq. (3). The average heat change $\mathcal{Q}(t)$ can be easily derived employing the first law of thermodynamics in Eq. (2). We have used the parameters indicated in Fig. 3 and our choice of frequencies has followed two important criteria: we need to clearly distinguish the two avoided levels in order to perform the jump, but at the same time we must avoid any degeneracy with other possible resonances in order to prevent unwanted heat flows that could reduce the efficiency. Our results can be found in Fig. 3.

We now discuss our findings. Once the dynamics start, a transient phase occurs in which both walls absorb thermal excitations from their own baths. However, while the interaction between W1 and the cavity converts part of the thermal phonons into photons, W2, which is momentarily not interacting with the cavity, thermalizes. In Fig. 3(a), $\Delta\mathcal{U} = 0$ corresponds to the energy of the system at the end of this transient phase. Recall that thermalization of the cavity while interacting with W1 is defined as stroke (I). During stroke (II), i.e., during compression, the cavity absorbs work from the drive and increases $\tilde{\omega}_{c,1}$ to $\tilde{\omega}_{c,2}$, eventually starting to absorb thermal excitations from the hot wall and converting them into photons [which defines stroke (III)]. This causes a drastic enhancement of the photon population at the expense of part of the phonon population, as seen in Fig. 3(b). At the same time, the population of the cold wall, now off resonance, increases and W1 thermalizes completely. Once the internal energy becomes constant and the populations stop fluctuating,

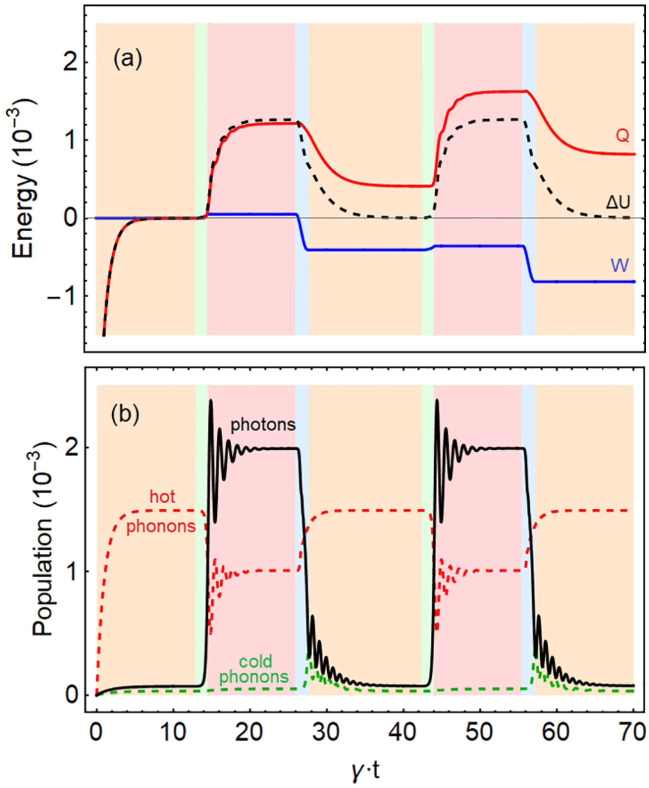

FIG. 3. Time evolution of the quantities of interest. (a) Variation of internal energy $\Delta\mathcal{U}$ (dashed, black), the work $\mathcal{W}$ (blue), and the heat $\mathcal{Q}$ (red). (b) Population of the cavity photon (black), the cold wall 1 phonons (dashed green), and the hot wall 2 phonons (dashed red). The background colors indicate the four stokes shown in Fig. 1: cold isochoric (orange), adiabatic compression (green), hot isochoric (red), and adiabatic expansion (blue). Here $\omega_1 = 2$, $\omega_2 = 2.6$, $\tilde{\omega}_{c,1} = 1.01$, $\tilde{\omega}_{c,2} = 1.31$, $g_1 = g_2 = 0.05$, $T_c = 0.15$, $T_h = 0.40$, $\gamma_1 = \gamma_2 = \gamma = 0.01$, $\kappa = 10^{-6}$, and $T_0 = 10^{-7}$. Frequencies and temperatures are normalized with respect to $\omega_{c,1}$.

we perform the rapid expansion of the cavity as described in stroke (IV), which causes the system to release an amount of energy which is higher than the one initially absorbed, a key feature of a properly functioning heat engine. This net gain becomes evident by looking at $\mathcal{W}$ in Fig. 3(a). After this last stroke, the cavity thermalizes with W1 again and the system reaches its initial configuration: a new cycle can now take place. We conclude that, after each cycle, we can extract a net amount of work using our system. An analysis of the efficiency is presented in the next section.

We now provide a few remarks on our proposal. As mentioned before we note that, once the resonance with the wall j is implemented, the interaction between wall j and the cavity mode is given by terms $(\hat{a}^\dagger)^2\hat{b}_j + \hat{a}^2\hat{b}_j^\dagger$ in $\hat{H}_I$, which mediate the phonon-photon conversions. Therefore, during the isochoric transformation the change in photon population is not a direct consequence of the thermalization of the cavity mode with the relative bath; instead it is a consequence of the partial conversion of thermal phonons into photon pairs. This process continues until the system wall cavity reaches the steady state, as can be observed in Fig. 3(b). Thus the number of photons at the end of any isochoric process will be less than $N = (e^{\omega_c/T_i} - 1)^{-1}$, with $i = \mathrm{c, h}$, as predicted by Bose-Einstein statistics and expected in the Otto cycle with a single mode as working substance [65,66]. In particular, the photon population in Fig. 3(b) can be compared with the average number of photons for a single cavity mode with frequency $\tilde{\omega}_{c,1} = 1.01$ and temperature $T_c = 0.15$, which is $N = 1.2 \times 10^{-3}$, and the population of a single-cavity mode with frequency $\tilde{\omega}_{c,2} = 1.31$ and temperature $T_h = 0.4$, which is $N = 3.96 \times 10^{-2}$. It can be seen that the photon population in our system is about 94% less than what was expected by a direct thermalization with the bath at the end of the cold isochoric and about 95% less at the end of the hot isochoric.

Furthermore, we notice that, during the isochoric strokes, quantum excitations are extracted from the thermal fluctuations of the walls and converted into photons without requiring the walls to perform any classical motion. This is in contrast to the semiclassical description of our setup, wherein walls are treated as classical degrees of freedom [36]. The phonon-photon conversion occurs between two quantum channels by simply activating the resonance $\omega_i = 2\omega_{c,i}$ $(i = 1, 2)$. The possibility of extracting thermal excitations from the walls in case of no coherent motion is a consequence of the fact that the two mirrors operate in the quantum regime [34,67].

Finally, we stress that, in contrast to other works studying optomechanical systems in a quantum thermodynamic framework [13,14], we employ a nonlinear Hamiltonian that includes the nonlinear interaction between the movable walls and the electromagnetic mode. Similar nonlinear Hamiltonians have recently started to acquire a dominant role in the interplay between optomechanics and quantum thermodynamics [68]. In our case, the entire dynamics of the system is based on the resonant conversion of phonons into photons and vice versa. To our knowledge, this effect has never been considered in a quantum thermodynamic context. This highlights the importance of moving beyond the linearized regime.

B. Analysis of the efficiency

In order to check the relation between efficiency and power, we first studied the efficiency of our device by fixing the frequency of the cold wall W1 and varying the frequency of the hot wall W2. It is crucial to stress that any modification to the frequency of one wall automatically leads to a change of the effective frequency of the cavity mode (it must be resonant to guarantee the energy flows) and consequently it also leads to a change of the interaction coupling constant, since the coupling strength g_j linearly depends on the frequency of the cavity mode [see Eq. (A10)]. Due to the complexity of the interactions between the various subsystems, together with the fact that only the two walls (and not the cavity mode) are constantly coupled with the heat baths, an analytical description of the dynamics is extremely difficult to carry out without significant approximations. For these reasons, we opted for a numerical investigation.

Concretely, we varied the frequency of the hot wall from 2.4 to 2.9 with a step of 0.1 and, for every value, we solved the master equation in Eq. (B1) for a single cycle in order to study the dynamics of the quantities of interest. Except for ω_2, we employed the same parameter as in Fig. 3 of the main text. The results of these simulations are resumed in Table I.

TABLE I. Trend of both the extracted work and the efficiency of the quantum heat engine for different frequency ω_2.

Frequency ω_2	$\mathcal{W}^{\text{out}}$ (10^{-4})	η
2.4	−4.04	0.223
2.5	−4.19	0.281
2.6	−4.07	0.334
2.7	−3.80	0.384
2.8	−3.44	0.431
2.9	−3.06	0.475

TABLE II. Trend of both the extracted work and the efficiency of the quantum heat engine for different values of the coupling constant.

Coupling g	$\mathcal{W}^{\text{out}}$ (10^{-4})	η
0.1	−3.65	0.317
0.2	−4.51	0.311
0.3	−4.55	0.302
0.4	−4.39	0.291
0.5	−4.19	0.281

Beyond the value $\omega_2 = 2.6$ we observe that the efficiency of the engine increases by enhancing ω_2, at the price of the output work. On the other hand, at $\omega_2 = 2.4$ we observe that the engine generates more power, but wastes a higher amount of energy in terms of dissipated heat. This is due to the fact that reducing the frequency of the hot wall also means diminishing both the frequency of the cavity mode and the wall-cavity coupling. The reduction of both cavity and wall frequencies leads to a lowering of the spacing of the eigenvalues, causing a general increase of the internal energy. The system therefore absorbs more heat from the environment during the thermalization and it is consequently capable of releasing more power. However, the lower coupling between the wall and the cavity inhibits the internal flows of energy and facilitates the exchange with the hot bath. The final effect is that, during the hot isochoric, the internal energy of the system enhances; the system therefore provides more work during the adiabatic expansion, but due to the lower wall-cavity coupling, it also dissipates a higher amount of energy in the form of heat.

Nevertheless, the engine can reach a maximum value of the output work at $\omega_2 = 2.5$, at which it reaches the efficiency $\eta = 0.281$. This efficiency is less than the Curzon-Ahlborn efficiency [69], which in our case reads $\eta_{\text{CA}} = 1 - \sqrt{T_c/T_h} = 0.388$. One of the main causes of this discrepancy is that the engine performs a sudden frequency switch during the adiabatic transformation [65]. In any case, we observe an increase of both the efficiency and the extracted work by decreasing the coupling constants g_1 and g_2. Results of numerical simulations are shown in Table II, where we conventionally fixed $g_1 = g_2 = g$. A reasonable explanation of this trend is that, in the strong coupling regime, excitations tend to be exchanged back and forth between the cavity mode and the wall, thereby attenuating the release of energy during the expansion. On the other hand, lower couplings allow excitations to easily leave the system, reducing this friction. However, although the efficiency increases further with lower gain, we also observe a drastic reduction of the extracted work once approaching the weak coupling regime. This result is expected for two reasons: on the one hand, simply because a low coupling inhibits the interaction between the subsystems and, consequently, the necessary heat flow to power the engine. On the other, because in the weak coupling regime the particle flow between the wall and the environment overcomes that between the optical and the mechanical modes, therefore slowing down the intermode heat transfer.

Finally, we want to discuss the role of the counter-rotating terms on the efficiency. To see whether their presence affects the performance of the heat engine, we carry out a simulation of the thermodynamic cycle by employing the following Hamiltonian:

$$\begin{aligned}\hat{H}_{\text{I}} =& \frac{g_1}{2}(\hat{a}^\dagger\hat{a} + \hat{a}\,\hat{a}^\dagger)(\hat{b}_1 + \hat{b}_1^\dagger) + \frac{g_1}{2}(\hat{a}^\dagger)^2\hat{b}_1 + \frac{g_1}{2}\hat{a}^2\hat{b}_1^\dagger \\ &+ \frac{g_2}{2}(\hat{a}^\dagger\hat{a} + \hat{a}\,\hat{a}^\dagger)(\hat{b}_2 + \hat{b}_2^\dagger) + \frac{g_2}{2}(\hat{a}^\dagger)^2\hat{b}_2 + \frac{g_2}{2}\hat{a}^2\hat{b}_2^\dagger,\end{aligned} \tag{4}$$

where the counter-rotating terms have been removed.

Employing the same parameters as in Fig. 3, the efficiency of the engine excluding the counter-rotating terms is $\eta = 0.325$, namely slightly less than the efficiency reported in Table I, $\eta = 0.334$. A reasonable explanation of this small discrepancy is the following: since the engine is working in the strong coupling regime, any interaction within the system is favored compared to the interaction with the environment. Albeit only at higher orders, counter-rotating terms contribute to the internal interactions between the cavity mode and the single walls via virtual processes. Therefore, the presence of counter-rotating terms facilitates the inner energy transfer between the single wall and the cavity mode within a unit of time and consequently it slightly inhibits the heat flows with the baths, therefore amplifying the power of the engine.

IV. CONCLUSIONS

In this work we proposed a quantum heat engine based on a cavity system composed of a scalar field trapped by two fluctuating walls that performs an Otto cycle. In our setup, we exploit the phonon-photon conversion mechanism to let the working substance exchange heat with the thermal baths during the cycle. We demonstrated that it is possible to extract net work using carefully modulated resonances and we have evaluated the overall efficiency of the cycle. We believe that this work opens the way to the systematic study of quantum field thermodynamic engines, to be used for fundamental science, as well as the development of novel quantum technologies.

ACKNOWLEDGMENTS

A.F. thanks the research center RIKEN for the hospitality. A.F. acknowledges the “JSPS Summer Program 2022” and the “FY2022 JSPS Postdoctoral Fellowship for Research in Japan (Short-term),” sponsored by the Japanese Society for the Promotion of Science (JSPS). F.K.W., A.F., and D.E.B. acknowledge support from the joint project No. 13N15685 “German Quantum Computer based on Superconducting Qubits (GeQCoS)” sponsored by the German Federal Ministry of Education and Research (BMBF) under the framework Quantum technologies—from basic research to the market. F.N. is supported in part by Nippon Telegraph and Telephone Corporation (NTT) Research, the Japan Science and Technology Agency (JST) [via the Quantum Leap Flagship Program (Q-LEAP) and the Moonshot R&D Grant No. JPMJMS2061], the Asian Office of Aerospace Research and Development (AOARD) (via Grant No. FA2386-20-1-4069), and the Foundational Questions Institute Fund (FQXi) via Grant No. FQXi-IAF19-06.

APPENDIX A: DERIVATION OF THE HAMILTONIAN

The literature shows different ways to derive the Hamiltonian of the system. A possible starting point could be the classical equation of motion of both the cavity and the two walls using time-dependent boundary conditions, as done by Law in [31]. However, in this section we show how to derive the Hamiltonian of the system from first principles employing the protocol in [34]. This procedure is based on the idea that the position of a nonfixed wall undergoes a fluctuation described by a quantum harmonic oscillator. This concept avoids the treatment of the problem starting from dynamical equations, since a real (classical) motion of the wall would occur only in the presence of coherence.

We start from the Lagrangian density of a massless scalar field in $(3+1)$ dimension:

$$\mathcal{L}(t,\mathbf{x}) = \tfrac{1}{2}\partial_\mu\phi\partial^\mu\phi. \tag{A1}$$

The equation of motion of such Lagrangian density with static Dirichlet boundary conditions is the Klein Gordon equation $\partial_t^2\phi - \nabla^2\phi=0$, which can be solved by any scalar field of the form

$$\phi(t,\mathbf{x}) = \sum_{\mathbf{n}}[\alpha_{\mathbf{n}}\,\phi_{\mathbf{n}}(t,x) + \alpha_{\mathbf{n}}^*\,\phi_{\mathbf{n}}^*(t,x)], \tag{A2}$$

with modes

$$\phi_{\mathbf{n}}(t,\mathbf{x}) = \sqrt{\frac{4}{\omega_{\mathbf{n}}V}}e^{-i\omega_{\mathbf{n}}t}\,\chi_{\mathbf{n}}(\mathbf{x}), \tag{A3}$$

where

$$\chi_{\mathbf{n}}(\mathbf{x}) = \sin\left(\frac{n_x\pi}{L_x}x\right)\sin\left(\frac{n_y\pi}{L_y}y\right)\sin\left(\frac{n_z\pi}{L_z}z\right), \tag{A4}$$

and the dispersion law reads

$$\omega_{\mathbf{n}} := \sqrt{\left(\frac{n_x\pi}{L_x}\right)^2 + \left(\frac{n_y\pi}{L_y}\right)^2 + \left(\frac{n_z\pi}{L_z}\right)^2}, \tag{A5}$$

with $\mathbf{n} \equiv (n_x, n_y, n_y)$ a set of positive integer numbers and box having volume $V = L_xL_yL_z$ [70]. With the typical formalism, well known from field theory, we can calculate the Hamiltonian density $\mathcal{H}(t,\mathbf{x}) = \frac{1}{2}\{\Pi^2(t,\mathbf{x}) + [\nabla\phi(t,\mathbf{x})]^2\}$, with canonical momentum $\Pi(t,\mathbf{x}) := -\partial_t\phi(t,\mathbf{x})$.

Hence the protocol consists of the following four steps.

(i) Extension of the box length with respect to L_x: $L_x \to L_x + \Delta L_x$, where $\Delta L_x/L_x \ll 1$, and Taylor expansion of $\mathcal{H}(t,\mathbf{x})$ up to the first order in $\Delta L_x/L_x$.

(ii) Spatial integration of the Hamiltonian density in volume V, thereby obtaining the classical Hamiltonian $H := \int \mathcal{H}\,dV$.

(iii) Quantization of the field Fourier coefficients $\alpha_{\mathbf{n}}$:

$$\alpha_{\mathbf{n}} \to \hat{a}_{\mathbf{n}},$$
$$\alpha_{\mathbf{n}}^* \to \hat{a}_{\mathbf{n}}^\dagger,$$

which now fulfill the standard commutation rules $[\hat{a}_{\mathbf{n}}, \hat{a}_{\mathbf{n}'}^\dagger] = \delta_{\mathbf{nn}'}$. We now need to quantize also the position of the two walls. If we assume that our system has a cylindrical symmetry along the x axis and that in our frame of reference the wall 1 is always at $x=0$, the second wall undergoes a fluctuation characterized by two Fourier harmonics: $\Delta L_x = \Delta L_1 + \Delta L_2$. Such harmonic fluctuations do not interact with each other and can be treated as two independent harmonic oscillators. Therefore, the quantization of such degrees of freedom leads to

$$\Delta L_1 \to \delta L_1(\hat{b}_1^\dagger + \hat{b}_1), \tag{A6}$$

$$\Delta L_2 \to \delta L_2(\hat{b}_2^\dagger + \hat{b}_2), \tag{A7}$$

where we introduced the annihilation and creation operators of two quantum harmonic oscillators fulfilling the standard commutation relations: $[\hat{b}_1, \hat{b}_1^\dagger] = [\hat{b}_2, \hat{b}_2^\dagger] = 1$, while all other commutators vanish. We notice that δL_1 and δL_2 are the zero-point fluctuations of two harmonic oscillators having different masses [40].

(iv) As a last step, we rewrite the quantum Hamiltonian $\hat{H}$ in normal order and we introduce two dimensionless amplitudes $\epsilon_1 := \delta L_1/L_x \ll 1$ and $\epsilon_2 := \delta L_2/L_x \ll 1$.

In the end, this procedure yields the Hamiltonian

$$\hat{H}_{\mathrm{s}} = \hat{H}_0 + \hat{H}_{\mathrm{I}}, \tag{A8}$$

where each term reads

$$\begin{aligned}\hat{H}_0 &:= \sum_{\mathbf{n}}\omega_{\mathbf{n}}\,\hat{a}_{\mathbf{n}}^\dagger\hat{a}_{\mathbf{n}} + \omega_1\hat{b}_1^\dagger\hat{b}_1 + \omega_2\hat{b}_2^\dagger\hat{b}_2,\\ \hat{H}_{\mathrm{I}} &:= 2\sum_{\mathbf{n}}\Bigg[\frac{k(n_y)^2 + k(n_z)^2}{\omega_{\mathbf{n}}}\hat{a}_{\mathbf{n}}^\dagger\hat{a}_{\mathbf{n}}\\ &\qquad -2\sum_{m_x}(-1)^{n_x+m_x}\frac{k(n_x)k(m_x)}{\sqrt{\omega_{\mathbf{n}}\,\omega_{m_x,n_y,n_z}}}\hat{X}_{\mathbf{n}}\hat{X}_{m_x,n_y,n_z}\Bigg]\\ &\qquad \times\,(\epsilon_1\hat{X}_{\mathrm{b}1} + \epsilon_2\hat{X}_{\mathrm{b}2}).\end{aligned} \tag{A9}$$

In order to simplify the notation, we introduced the wave vector $k(n_w) = \pi n_w/L_w$, with $w = x, y, z$, the quadrature position operators $\hat{X}_{\mathrm{b},j} = \frac{1}{2}(\hat{b}_j^\dagger + \hat{b}_j)$, with $j = 1, 2$, and $\hat{X}_{\mathbf{n}} = \frac{1}{2}(\hat{a}_{\mathbf{n}}^\dagger + \hat{a}_{\mathbf{n}})$. We note that the ambiguity on the negative sign in $\hat{H}_{\mathrm{I}}$ is solved by including all terms of the Taylor expansion with respect to δL [31].

For our purposes, such Hamiltonian can be drastically simplified by assuming the following.

(1) The constraint $L_x \gg L_y, L_z$ on the magnitude of the length of the edges of the piston. This is motivated by the fact that there are no excitations initially present in the y and z degrees of freedom. Given the higher energy required to excite these degrees of freedom (since the energy gaps are inversely proportional to the corresponding length) it is reasonable to assume that they will remain unexcited. Thus we can drop the first term in the square brackets and obtain Hamiltonian (1) in the main text.

(2) The presence of only one cavity mode, say the fundamental mode $\omega_{1,1,1} = \omega_c$. This is a reasonable assumption, since other cavity modes with $n_x > 1$ are initialized in the vacuum state.

Under such assumptions, the system Hamiltonian is reduced to Eq. (1) of the main text, where

$$g_j = -\epsilon_j \frac{k(n_x)^2}{2\omega_{\mathbf{n}}}, \tag{A10}$$

with $j = 1, 2$ indicating the jth wall.

APPENDIX B: MASTER EQUATION IN THE DRESSED PICTURE AND THE DRESSED OPERATORS

In this section we want to review the necessary tools to describe the time evolution of the quantities of interest. Working in the Schrödinger picture, we first need to solve the master equation for the density operator; however, since we are dealing with a strongly interacting system, the best way to proceed is to employ the master equation in the dressed picture [50]. To do this, first let us introduce the transition amplitudes for the canonical position operators calculated on the dressed basis: $c_{ij} = \langle i|\hat{a} + \hat{a}^\dagger|j\rangle$, $u_{ij} = \langle i|\hat{b}_1 + \hat{b}_1^\dagger|j\rangle$, and $v_{ij} = \langle i|\hat{b}_2 + \hat{b}_2^\dagger|j\rangle$, where the state $|i\rangle$ is the ith eigenstate of the Hamiltonian with eigenenergy E_i.

We assume that the three subsystems are coupled to three different baths: in particular, the wall 1 is coupled to a cold bath with damping rate γ_1 and the wall 2 is coupled to a hot bath with damping rate γ_2. Finally, we also assume that the cavity always weakly interacts with its own bath at $T \simeq 0$, with damping rate $\kappa \simeq 0$. Although it does not play an active role in our dynamics, the interaction with the third bath whose temperature is not exactly zero is expected in experimental scenarios and prevents the violation of the third law of thermodynamics.

The master equation in the dressed picture has been obtained before [50,51] and it reads

$$\frac{d\hat{\rho}}{dt} = -i[\hat{H}, \hat{\rho}] + (\hat{\mathcal{L}}_c + \hat{\mathcal{L}}_u + \hat{\mathcal{L}}_v)\hat{\rho}, \tag{B1}$$

where we have defined

$$\hat{\mathcal{L}}_x\hat{\rho} = y \sum_{j,i>j} |x_{ij}|^2 \{n_{ij}(T)\mathcal{D}[\hat{P}_{ij}]\hat{\rho} + [1 + n_{ij}(T)]\mathcal{D}[\hat{P}_{ji}]\hat{\rho}\}, \tag{B2}$$

which needs to be supplemented by the quantities $x = c, u, v$, the rates of losses $y = \gamma_1, \gamma_2, \kappa$, the thermal excitation numbers $n_{ij}(T) = (e^{(E_i - E_j)/T} - 1)^{-1}$, the superoperators

$$\mathcal{D}[\hat{P}_{ij}]\hat{\rho} = \tfrac{1}{2}(2\hat{P}_{ij}\hat{\rho}\hat{P}_{ij}^\dagger - \hat{\rho}\hat{P}_{ij}^\dagger\hat{P}_{ij} - \hat{P}_{ij}^\dagger\hat{P}_{ij}\hat{\rho}), \tag{B3}$$

and the transition operators $\hat{P}_{ij} = |i\rangle\langle j|$.

In order to evaluate the quantity of interest, it is necessary to define a set of dressed annihilation operators for the various subsystems, and we have

$$\hat{A} = \sum_{j,i>j} c_{ij}\hat{P}_{ij}, \quad \hat{B}_1 = \sum_{j,i>j} u_{ij}\hat{P}_{ij}, \quad \hat{B}_2 = \sum_{j,i>j} v_{ij}\hat{P}_{ij}. \tag{B4}$$

We recall that the photon as well as the phonon population at any instant t of time is given by $N_c(t) = \mathrm{Tr}[\hat{A}^\dagger\hat{A}\rho(t)]$ and $N_{\mathrm{w}_j}(t) = \mathrm{Tr}[\hat{B}_j^\dagger\hat{B}_j\rho(t)]$ $(j = 1, 2)$, respectively.

APPENDIX C: EXTERNAL DRIVE

The total Hamiltonian includes a time-dependent term acting as an external drive that periodically shifts the effective frequency of cavity mode from $\tilde{\omega}_{c,1}$ to $\tilde{\omega}_{c,2}$ and backwards. From a physical perspective, the role of such external drive is to simulate the compression and the expansion of the cavity, thereby activating the resonant phonon-photon conversion with either $\tilde{\omega}_{c,1}$ or $\tilde{\omega}_{c,2}$. The explicit form of the time-dependent term is $\hat{H}_{\mathrm{dr}}(t) = f(t)\Delta\omega\hat{A}^\dagger\hat{A}$, where $\Delta\omega = \tilde{\omega}_{c,2} - \tilde{\omega}_{c,1}$, and $\hat{A}, \hat{A}^\dagger$ are the cavity dressed operators in Eq. (B4). The function $f(t)$ is a periodic smooth step function which allows us to rapidly vary the frequency of the cavity during the adiabatic transformations. Its explicit form is

$$\begin{aligned} f(t) = \sum_i^N &\{\sin^2[\Omega(t - t_i)]\theta[t - t_i] \\ &+ \sin^2[\Omega(t - t_i - \tau)]\theta[t - t_i - \tau] \\ &- \sin^2[\Omega(t - t_i - \Delta t)]\theta[t - t_i - \Delta t] \\ &- \sin^2[\Omega(t - t_i - \tau - \Delta t)]\theta[t - t_i - \tau - \Delta t]\}, \end{aligned} \tag{C1}$$

where t_i indicate the instants of time when the cycle is run, Δt is the duration of the hot isochoric, τ is the duration of the two adiabatics, and $\Omega = 2\pi/\tau$. $\theta[t]$ is the Heaviside function. The duration of the cold isochoric was estimated such that $\Delta\mathcal{U}$ reaches zero at the end of the transformation (see Fig. 3 of the main text) and it corresponds to $t_2 - t_1 - 2\tau - \Delta t$, whereas the duration of one cycle is $t_2 - t_1$.

We finally stress that, since the frequency change due to the external drive occurs much faster than the effective coupling, the system does not have time to modify its eigenstates, which implies that we do not need to diagonalize the Hamiltonian at all times. Therefore, we can maintain the same eigenbasis, hence the same dressed operators, throughout the whole dynamics. Moreover, the interaction between the cavity and each wall occurs not only at the minimum point of the level avoidance but also weakly in its proximity. It follows that this rapid jump between $\tilde{\omega}_{c,1}$ and $\tilde{\omega}_{c,2}$ is necessary to ensure the classical adiabaticity of the process [11], namely simulating the deactivation of the interaction between the cavity and the bath mediated by the wall. In this quantum description, the two walls are thermalized via different baths. In particular, the interaction between a specific bath and the cavity occurs once the resonance condition with the relative wall is imposed and it is halted once the system is driven off resonance. We have W2 at frequency ω_2 that thermalizes via a hot bath at T_{h}, while W1 has a lower frequency $\omega_1 < \omega_2$ and it is thermalized via a cold bath at $T_{\mathrm{c}} < T_{\mathrm{h}}$. The cavity interacts with its own bath at $T \simeq 0$.

[1] J. Gemmer, M. Michel, and G. Mahler, *Quantum Thermodynamics: Emergence of Thermodynamic Behavior within Composite Quantum Systems* (Springer, Berlin, 2009), Vol. 784.

[2] S. Vinjanampathy and J. Anders, Quantum thermodynamics, Contemp. Phys. **57**, 545 (2016).

[3] G. Kurizki and A. G. Kofman, *Thermodynamics and Control of Open Quantum Systems* (Cambridge University Press, Cambridge, UK, 2022).

[4] P. Skrzypczyk, A. J. Short, and S. Popescu, Work extraction and thermodynamics for individual quantum systems, Nat. Commun. **5**, 4185 (2014).

[5] J. P. Pekola, Towards quantum thermodynamics in electronic circuits, Nat. Phys. **11**, 118 (2015).

[6] M. Perarnau-Llobet, K. V. Hovhannisyan, M. Huber, P. Skrzypczyk, N. Brunner, and A. Acín, Extractable work from correlations, Phys. Rev. X **5**, 041011 (2015).

[7] M. O. Scully, M. S. Zubairy, G. S. Agarwal, and H. Walther, Extracting work from a single heat bath via vanishing quantum coherence, Science **299**, 862 (2003).

[8] Y. Ezzahri and K. Joulain, Vacuum-induced phonon transfer between two solid dielectric materials: Illustrating the case of Casimir force coupling, Phys. Rev. B **90**, 115433 (2014).

[9] J. B. Pendry, K. Sasihithlu, and R. V. Craster, Phonon-assisted heat transfer between vacuum-separated surfaces, Phys. Rev. B **94**, 075414 (2016).

[10] H. T. Quan, P. Zhang, and C. P. Sun, Quantum heat engine with multilevel quantum systems, Phys. Rev. E **72**, 056110 (2005).

[11] H. T. Quan, Y.-X. Liu, C. P. Sun, and F. Nori, Quantum thermodynamic cycles and quantum heat engines, Phys. Rev. E **76**, 031105 (2007).

[12] H. T. Quan, Quantum thermodynamic cycles and quantum heat engines. II, Phys. Rev. E **79**, 041129 (2009).

[13] K. Zhang, F. Bariani, and P. Meystre, Quantum optomechanical heat engine, Phys. Rev. Lett. **112**, 150602 (2014).

[14] K. Zhang, F. Bariani, and P. Meystre, Theory of an optomechanical quantum heat engine, Phys. Rev. A **90**, 023819 (2014).

[15] A. Mari, A. Farace, and V. Giovannetti, Quantum optomechanical piston engines powered by heat, J. Phys. B: At., Mol., Opt. Phys. **48**, 175501 (2015).

[16] M. Brunelli, A. Xuereb, A. Ferraro, G. D. Chiara, N. Kiesel, and M. Paternostro, Out-of-equilibrium thermodynamics of quantum optomechanical systems, New J. Phys. **17**, 035016 (2015).

[17] M. Kolář, A. Ryabov, and R. Filip, Extracting work from quantum states of radiation, Phys. Rev. A **93**, 063822 (2016).

[18] Z. Holmes, J. Anders, and F. Mintert, Enhanced energy transfer to an optomechanical piston from indistinguishable photons, Phys. Rev. Lett. **124**, 210601 (2020).

[19] P. Salamon, K. H. Hoffmann, Y. Rezek, and R. Kosloff, Maximum work in minimum time from a conservative quantum system, Phys. Chem. Chem. Phys. **11**, 1027 (2009).

[20] D. Stefanatos, Minimum-time transitions between thermal equilibrium states of the quantum parametric oscillator, IEEE Trans. Autom. Control **62**, 4290 (2017).

[21] S. Lee, M. Ha, and H. Jeong, Quantumness and thermodynamic uncertainty relation of the finite-time otto cycle, Phys. Rev. E **103**, 022136 (2021).

[22] M. Kloc, P. Cejnar, and G. Schaller, Collective performance of a finite-time quantum Otto cycle, Phys. Rev. E **100**, 042126 (2019).

[23] A. Das and V. Mukherjee, Quantum-enhanced finite-time Otto cycle, Phys. Rev. Res. **2**, 033083 (2020).

[24] J.-F. Chen, C.-P. Sun, and H. Dong, Achieve higher efficiency at maximum power with finite-time quantum Otto cycle, Phys. Rev. E **100**, 062140 (2019).

[25] V. Singh and O. E. Müstecaplıoğlu, Performance bounds of nonadiabatic quantum harmonic Otto engine and refrigerator under a squeezed thermal reservoir, Phys. Rev. E **102**, 062123 (2020).

[26] M. Campisi and R. Fazio, The power of a critical heat engine, Nat. Commun. **7**, 11895 (2016).

[27] M. Boubakour, T. Fogarty, and T. Busch, Interaction-enhanced quantum heat engine, Phys. Rev. Res. **5**, 013088 (2023).

[28] M. Gluza, J. Sabino, N. H. Y. Ng, G. Vitagliano, M. Pezzutto, Y. Omar, I. Mazets, M. Huber, J. Schmiedmayer, and J. Eisert, Quantum field thermal machines, PRX Quantum **2**, 030310 (2021).

[29] O. Di Stefano, A. Settineri, V. Macrì, A. Ridolfo, R. Stassi, A. F. Kockum, S. Savasta, and F. Nori, Interaction of mechanical oscillators mediated by the exchange of virtual photon pairs, Phys. Rev. Lett. **122**, 030402 (2019).

[30] K. Y. Fong, H.-K. Li, R. Zhao, S. Yang, Y. Wang, and X. Zhang, Phonon heat transfer across a vacuum through quantum fluctuations, Nature (London) **576**, 243 (2019).

[31] C. K. Law, Interaction between a moving mirror and radiation pressure: A Hamiltonian formulation, Phys. Rev. A **51**, 2537 (1995).

[32] S. Butera and R. Passante, Field fluctuations in a one-dimensional cavity with a mobile wall, Phys. Rev. Lett. **111**, 060403 (2013).

[33] V. Macrì, A. Ridolfo, O. Di Stefano, A. F. Kockum, F. Nori, and S. Savasta, Nonperturbative dynamical casimir effect in optomechanical systems: Vacuum Casimir-Rabi splittings, Phys. Rev. X **8**, 011031 (2018).

[34] A. Ferreri, H. Pfeifer, F. K. Wilhelm, S. Hofferberth, and D. E. Bruschi, Interplay between optomechanics and the dynamical Casimir effect, Phys. Rev. A **106**, 033502 (2022).

[35] W. Qin, V. Macrì, A. Miranowicz, S. Savasta, and F. Nori, Emission of photon pairs by mechanical stimulation of the squeezed vacuum, Phys. Rev. A **100**, 062501 (2019).

[36] V. Dodonov, Fifty years of the dynamical Casimir effect, Physics **2**, 67 (2020).

[37] D. E. Bruschi, Time evolution of coupled multimode and multiresonator optomechanical systems, J. Math. Phys. **60**, 062105 (2019).

[38] N. Friis, A. R. Lee, and J. Louko, Scalar, spinor, and photon fields under relativistic cavity motion, Phys. Rev. D **88**, 064028 (2013).

[39] M. Aspelmeyer, P. Meystre, and K. Schwab, Quantum optomechanics, Phys. Today **65**(7), 29 (2012).

[40] M. Aspelmeyer, T. J. Kippenberg, and F. Marquardt, Cavity optomechanics, Rev. Mod. Phys. **86**, 1391 (2014).

[41] A. D. O'Connell, M. Hofheinz, M. Ansmann, R. C. Bialczak, M. Lenander, E. Lucero, M. Neeley, D. Sank, H. Wang, M. Weides *et al.*, Quantum ground state and single-phonon control of a mechanical resonator, Nature (London) **464**, 697 (2010).

[42] J. R. Johansson, G. Johansson, C. M. Wilson, and F. Nori, Dynamical Casimir effect in superconducting microwave circuits, Phys. Rev. A **82**, 052509 (2010).

[43] C. Wilson, G. Johansson, A. Pourkabirian, M. Simoen, J. Johansson, T. Duty, F. Nori, and P. Delsing, Observation of the dynamical Casimir effect in a superconducting circuit, Nature (London) **479**, 376 (2011).

[44] J. R. Johansson, G. Johansson, and F. Nori, Optomechanical-like coupling between superconducting resonators, Phys. Rev. A **90**, 053833 (2014).

[45] E.-j Kim, J. R. Johansson, and F. Nori, Circuit analog of quadratic optomechanics, Phys. Rev. A **91**, 033835 (2015).

[46] R. Hab-arrih, A. Jellal, D. Stefanatos, and E. H. El Kinani, Virtual excitations and quantum correlations in ultra-strongly coupled harmonic oscillators under intrinsic decoherence, Optik **278**, 170719 (2023).

[47] B. Wang, J.-M. Hu, V. Macrì, Z.-L. Xiang, and F. Nori, Coherent resonant coupling between atoms and a mechanical oscillator mediated by cavity-vacuum fluctuations, Phys. Rev. Res. **5**, 013075 (2023).

[48] E. Russo, A. Mercurio, F. Mauceri, R. Lo Franco, F. Nori, S. Savasta, and V. Macrì, Optomechanical two-photon hopping, Phys. Rev. Res. **5**, 013221 (2023).

[49] H.-P. Breuer and F. Petruccione, *The Theory of Open Quantum Systems* (Oxford University Press on Demand, 2002).

[50] F. Beaudoin, J. M. Gambetta, and A. Blais, Dissipation and ultrastrong coupling in circuit QED, Phys. Rev. A **84**, 043832 (2011).

[51] A. Settineri, V. Macrì, A. Ridolfo, O. Di Stefano, A. F. Kockum, F. Nori, and S. Savasta, Dissipation and thermal noise in hybrid quantum systems in the ultrastrong-coupling regime, Phys. Rev. A **98**, 053834 (2018).

[52] T. Tanabe, M. Notomi, E. Kuramochi, A. Shinya, and H. Taniyama, Trapping and delaying photons for one nanosecond in an ultrasmall high-Q photonic-crystal nanocavity, Nat. Photon. **1**, 49 (2007).

[53] D. Armani, T. Kippenberg, S. Spillane, and K. Vahala, Ultra-high-q toroid microcavity on a chip, Nature (London) **421**, 925 (2003).

[54] Y. Zhang and M. Lončar, Ultra-high quality factor optical resonators based on semiconductor nanowires, Opt. Express **16**, 17400 (2008).

[55] S. Noda, M. Fujita, and T. Asano, Spontaneous-emission control by photonic crystals and nanocavities, Nat. Photon. **1**, 449 (2007).

[56] M. A. Sillanpää, J. I. Park, and R. W. Simmonds, Coherent quantum state storage and transfer between two phase qubits via a resonant cavity, Nature (London) **449**, 438 (2007).

[57] M. Hofheinz, E. Weig, M. Ansmann, R. C. Bialczak, E. Lucero, M. Neeley, A. O'connell, H. Wang, J. M. Martinis, and A. Cleland, Generation of Fock states in a superconducting quantum circuit, Nature (London) **454**, 310 (2008).

[58] M. Hofheinz, H. Wang, M. Ansmann, R. C. Bialczak, E. Lucero, M. Neeley, A. O'connell, D. Sank, J. Wenner, J. M. Martinis *et al.*, Synthesizing arbitrary quantum states in a superconducting resonator, Nature (London) **459**, 546 (2009).

[59] H. Wang, M. Mariantoni, R. C. Bialczak, M. Lenander, E. Lucero, M. Neeley, A. D. O'Connell, D. Sank, M. Weides, J. Wenner, T. Yamamoto, Y. Yin, J. Zhao, J. M. Martinis, and A. N. Cleland, Deterministic entanglement of photons in two superconducting microwave resonators, Phys. Rev. Lett. **106**, 060401 (2011).

[60] M. Mariantoni, H. Wang, R. C. Bialczak, M. Lenander, E. Lucero, M. Neeley, A. O'Connell, D. Sank, M. Weides, J. Wenner *et al.*, Photon shell game in three-resonator circuit quantum electrodynamics, Nat. Phys. **7**, 287 (2011).

[61] A. F. Kockum, V. Macrì, L. Garziano, S. Savasta, and F. Nori, Frequency conversion in ultrastrong cavity qed, Sci. Rep. **7**, 5313 (2017).

[62] S. Qvarfort, M. R. Vanner, P. F. Barker, and D. E. Bruschi, Master-equation treatment of nonlinear optomechanical systems with optical loss, Phys. Rev. A **104**, 013501 (2021).

[63] F. Schneiter, S. Qvarfort, A. Serafini, A. Xuereb, D. Braun, D. Rätzel, and D. E. Bruschi, Optimal estimation with quantum optomechanical systems in the nonlinear regime, Phys. Rev. A **101**, 033834 (2020).

[64] S. Qvarfort, A. Serafini, A. Xuereb, D. Braun, D. Rätzel, and D. E. Bruschi, Time-evolution of nonlinear optomechanical systems: interplay of mechanical squeezing and non-gaussianity, J. Phys. A: Math. Theor. **53**, 075304 (2020).

[65] O. Abah, J. Roßnagel, G. Jacob, S. Deffner, F. Schmidt-Kaler, K. Singer, and E. Lutz, Single-ion heat engine at maximum power, Phys. Rev. Lett. **109**, 203006 (2012).

[66] J. Roßnagel, O. Abah, F. Schmidt-Kaler, K. Singer, and E. Lutz, Nanoscale heat engine beyond the Carnot limit, Phys. Rev. Lett. **112**, 030602 (2014).

[67] A. Settineri, V. Macrì, L. Garziano, O. Di Stefano, F. Nori, and S. Savasta, Conversion of mechanical noise into correlated photon pairs: Dynamical Casimir effect from an incoherent mechanical drive, Phys. Rev. A **100**, 022501 (2019).

[68] M. Izadyari, M. Öncü, K. Durak, and Ö. E. Müstecaplıoğlu, Quantum signatures in a quadratic optomechanical heat engine with an atom in a tapered trap, J. Opt. Soc. Am. B **39**, 3247 (2022).

[69] F. L. Curzon and B. Ahlborn, Efficiency of a Carnot engine at maximum power output, Am. J. Phys. **43**, 22 (1975).

[70] M. Crocce, D. A. R. Dalvit, and F. D. Mazzitelli, Resonant photon creation in a three-dimensional oscillating cavity, Phys. Rev. A **64**, 013808 (2001).